Rogue-wave pattern transition induced by relative frequency

Li-Chen Zhao,* Guo-Guo Xin, and Zhan-Ying Yang
Department of Physics, Northwest University, Xi'an 710069, China
(Received 17 April 2014; published 28 August 2014)

We revisit a rogue wave in a two-mode nonlinear fiber whose dynamics is described by two-component coupled nonlinear Schrödinger equations. The relative frequency between two modes can induce different rogue wave patterns transition. In particular, we find a four-petaled flower structure rogue wave can exist in the two-mode coupled system, which possesses an asymmetric spectrum distribution. Furthermore, spectrum analysis is performed on these different type rogue waves, and the spectrum relations between them are discussed. We demonstrate qualitatively that different modulation instability gain distribution can induce different rogue wave excitation patterns. These results would deepen our understanding of rogue wave dynamics in complex systems.

DOI: 10.1103/PhysRevE.90.022918 PACS number(s): 05.45.Yv, 42.65.Tg, 42.81.Dp

I. INTRODUCTION

Recent experiments on rogue waves (RWs) suggest that the unique wave arises from modulational instability, and the rational solution of a nonlinear Schrödinger equation (NLSE) can be used to describe dynamics of RWs prototypically [1–3]. Based on the rational solutions, it has been found that there are some interesting patterns for RWs [4,5]. The fundamental RW of scalar NLSE has the well-known eye-shaped structure [6]. A dark RW is found to have an anti-eye-shaped structure in a two-component coupled NLSE [7]. A four-petaled flower structure RW was reported very recently in a three-component coupled system [8,9]. Then, can the four-petaled flower structure pattern exist in a two-component coupled NLSE? Are there any relations between these different types of RW patterns? The pattern types of RWs still need further research, since they would provide knowledge or information on RW excitation and application in many nonlinear systems (nonlinear fiber, financial system, Bose-Einstein condensate, plasma, etc.).

Since RWs have been excited widely in nonlinear fiber systems [1,10,11], we choose a nonlinear fiber system to discuss the above questions. For a single-mode optical fiber, the frequency of the background field has no real effects on the pattern structure for RWs, since the corresponding solutions can be correlated through a trivial Galileo transformation. But for coupled mode fiber, the relative frequency between different mode fields has real physical effects and cannot be erased by any trivial transformation. Modulational instability (MI) analysis of a continuous wave background suggests that the relative frequency has a real effect on the instability spectrum properties (see Fig. 4). We expect that the RW excitation pattern could be changed with varying relative frequency.

In this paper, we find a four-petaled flower structure RW in the two-component coupled nonlinear Schrödinger equation, in contrast to the eye-shaped, anti-eye-shaped one reported previously [6,7]. Furthermore, we demonstrate that these RW patterns can be transited to each other through varying the relative frequency between the two modes in nonlinear fiber. Moreover, their spectra are characterized exactly and compared in detail. This provides a qualitative way to understand the relations between these different types of patterns of vector RWs and would enrich our knowledge about RW dynamics in complex systems.

II. THE SINGLE RW SOLUTION WITH ARBITRARY RELATIVE FREQUENCY

For a two-mode nonlinear fiber, the wave evolution dynamics can be described by the following two-coupled NLSE in dimensionless form:

$$i\frac{\partial\psi_1}{\partial z}+\frac{\partial^2\psi_1}{\partial t^2}+2[|\psi_1|^2+|\psi_2|^2]\psi_1=0, \tag{1}$$

$$i\frac{\partial\psi_2}{\partial z}+\frac{\partial^2\psi_2}{\partial t^2}+2[|\psi_1|^2+|\psi_2|^2]\psi_2=0, \tag{2}$$

where ψ_1 and ψ_2 are the two mode optical fields. z denotes the evolution dimension, and t represents the temporal distribution dimension for the wave fields. The related dispersion coefficient and Kerr nonlinearity strength have been scaled to be 1 and 2 through coordinates transformation. The coupled partial equations can also be used to describe the dynamics of a matter wave in a quasi-onedimensional two-component Bose-Einstein condensate [12], the evolution of optical fields in a two-mode or polarized nonlinear fiber [13], and even the vector financial system [14]. Equation (1) has been solved to get nonlinear localized waves on the nontrivial seed solutions [7,15,16]. They presented some interesting localized wave dynamics in the coupled model, such as that RWs interact with a bright-dark soliton [15,16], dark RW [7], and double RW [7]. In this paper we revisit RWs in the coupled system. To discuss the effects of background fields on RW dynamics, we consider the generalized continuous wave background as

$$\psi_{10}=s_1\exp\left[i\left(2s_1^2+2s_2^2\right)z\right], \tag{3}$$

$$\psi_{20}=s_2\exp\left[ikt+i\left(2s_1^2+2s_2^2-k^2\right)z\right], \tag{4}$$

where s_1 and s_2 are two arbitrary real constants and denote the background amplitude. Since the relative frequency plays a real physical effect on the dynamics of a localized wave, we introduce the parameter k to denote the frequency difference of the continuous wave backgrounds in the two modes.

*zhaolichen3@163.com

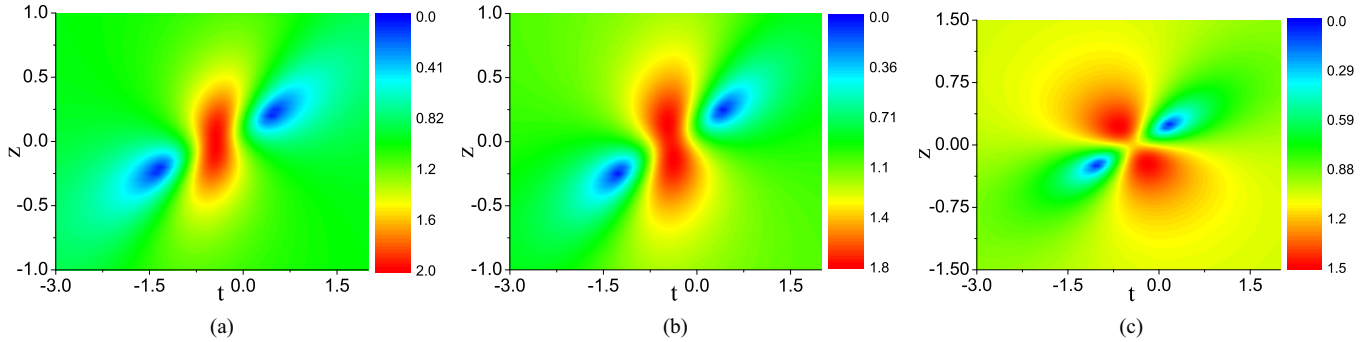

FIG. 1. (Color online) The process for which an eye-shaped RW transits to be a four-petaled flower structure RW in the component $|\psi_2|$ with varying the relative frequency. (a) With $k = 0.999$, (b) $k = 1.01$, and (c) $k = 1.1$. The other parameters are $s_1 = 1, s_2 = 1, A_3 = 3$.

With some constrains on frequencies of the two modes, we have derived a double RW and four fundamental RWs in the coupled model [7,17]. However, the constraint conditions would limit the pattern types of RWs greatly in the model. To study the patten types of fundamental RWs conveniently, we release the constraint condition to derive a more general single RW solution. With arbitrary relative frequency k, the rational solution corresponding to a single RW can be written as

$$\psi_1 = \left[1 - \frac{i(\lambda - \lambda^*)\Phi_1\Phi_2^*/s_1}{|\Phi_1|^2 + |\Phi_2|^2 + |\Phi_3|^2}\right]\psi_{10}, \tag{5}$$

$$\psi_2 = \left[1 - \frac{i(\lambda - \lambda^*)\Phi_1\Phi_3^*/s_2}{|\Phi_1|^2 + |\Phi_2|^2 + |\Phi_3|^2}\right]\psi_{20}, \tag{6}$$

where the $*$ means the complex conjugate, and the explicit expressions for Φ_j $(j = 1,2,3)$ are presented in the Appendix. Four essential parameters determine the explicit dynamics of RW: s_1, s_2, A_3, and k. The solution can be used to observe the effects of these parameters on RW dynamics through the control variate method. Interestingly, we find the relative frequency plays an essential role in determining the structure profile with other parameters unchanged. For example, we set $s_1 = s_2 = s$ to observe the effects of relative frequency on RW pattern dynamics, with $\lambda = \frac{\sqrt{k^6 - 4k^2[5k^2s^2 - 2\sqrt{-s^2(k^2-s^2)^3} + 2s^4]} - k^3}{2k^2}$. The other cases can be discussed directly through varying parameters in the general single RW solution. We find that the transition process of different RW patterns can be observed by varying the relative frequency. In particular, we demonstrate that the four-petaled flower structure RW can exist in a two-component coupled NLS model, which was reported previously in three-component coupled nonlinear systems [8,9].

III. THE ROGUE WAVE PATTERN TRANSITION INDUCED BY THE RELATIVE FREQUENCY

To demonstrate the transition process, we observe a RW pattern with varying the relative frequency from low to high. When $k < 0$, the structure evolution characters are similar to the ones $k > 0$; just the temporal velocity of the RW is the inverse. The structure is mainly determined by the absolute value of k. When $k < 1$ s, RWs in the two components both are eye-shaped ones, which are identical to the ones in Fig. 1 in Ref. [15]. For an example, we show the evolution structure of a RW in component ψ_2 of a case with $k = 0.999$ s in Fig. 1(a). It should be pointed that when $k = 1$ s, the solution form fails to present RW dynamics, and we need resolve it. In this case, there are two eye-shaped ones or two with different patterns in each component, which have been shown in Ref. [7]. However, their pattern types are very complicated to be classified. Here the fundamental RW pattern types are discussed conveniently and clearly. When k is a bit bigger than s, the RW pattern in component ψ_1 is still an eye-shaped one (we do not show it hereafter), but the RW pattern in ψ_2 begins to change. Namely, the hump of an eye-shaped one will split to be two on the temporal-spatial distribution. As an example, we demonstrate one case with $k = 1.01$ s in Fig. 1(b). It is seen that there are two humps emerging and the humps are not isolated in this case. Interestingly, the humps can be isolated with each other when k is much larger. When $k = 1.1$ s, the distance between two humps becomes much larger, for which the two humps can be seen as isolated. The structure seems like a four-petaled flower, which is very similar to the one found in the three-component case [8]. The evolution character is quite different from the eye-shaped RW reported before, which possesses one hump and two valleys [6,18–21]. In this way, we demonstrate a symmetric eye-shaped RW transit to be a four-petaled flower RW in component ψ_2 through increasing k from 0 to a bit larger than 1 s.

We observe the transition from four-petaled flower one to anti-eye-shaped one through increasing the relative frequency further. When $k = 1.3$ s, the two humps become much more isolated, and the two valleys begin to approach each other significantly, as shown in Fig. 2(a). When $k = 1.5$ s, the two valleys approach each other further and tend to merge [Fig. 2(b)]. When $k = 1.8$ s, the two valleys merge to be one valley in component ψ_2, which makes the RW possess an anti-eye structure [Fig. 2(c)], which is identical with the dark RW reported in Ref. [7]. The RW pattern in ψ_1 just changes its size, and the eye-shaped character is kept fundamentally during the whole transition process.

IV. SPECTRUM ANALYSIS OF DIFFERENT ROGUE WAVE PATTERNS

Spectrum anlysis of a Peregrine RW suggests that it has a specific triangular spectrum, which could be used for early warning of RWs through spectral measurements [22]. Recently, intensity and phase spectral shaping was used to

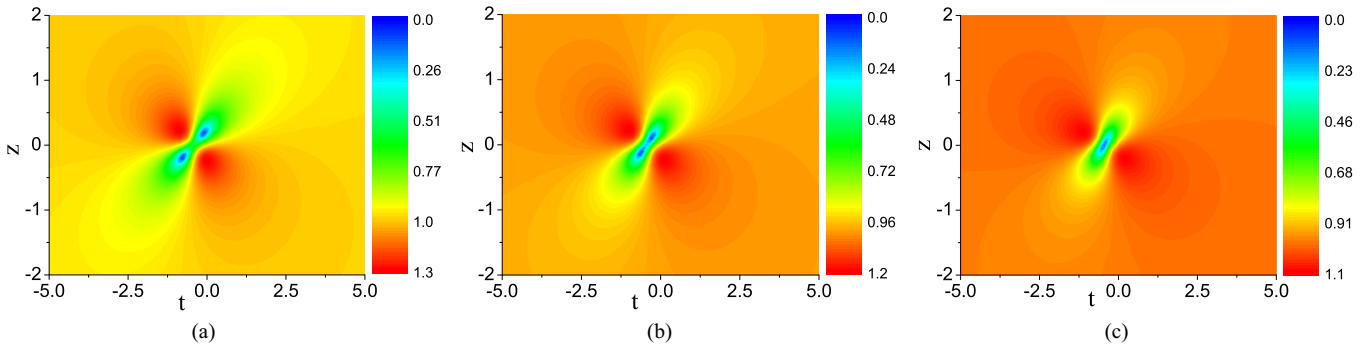

FIG. 2. (Color online) The process for which a four-petaled flower structure RW transits to be an anti-eye-shaped RW in the component ψ_2 with varying the relative frequency. (a) With $k = 1.3$, (b) $k = 1.5$ (c) $k = 1.8$. The other parameters are $s_1 = s_2 = 1, A_3 = 3$.

generate RWs successfully in a nonlinear fiber [23]. Therefore, the spectrum analysis is meaningful for RW prediction and excitation research [23,24]. Then we perform spectrum analysis of these RW discussed above through the following Fourier transformation:

$$F_{1,2}(\omega,z) = \frac{1}{\sqrt{2\pi}} \int_{-\infty}^{+\infty} \psi_{1,2}(t,z) \exp[i\omega t]\, dt. \qquad (7)$$

The solution can be written in the form of a constant background plus a signal. The constant background is infinity, and thus its integral is $\delta(\omega - \omega_0)$; then we can eliminate the δ function and obtain the spectrum of the RW signal. When $k = 1.1\ s$, the signal will evolve to be the four-petaled flower structure RW in Fig. 1(c). The corresponding spectrum evolutions of a RW in component ψ_1 and ψ_2 are shown in Fig. 3(a) and 3(b), respectively. There is a valley on the lower frequency and a hump on the higher frequency, compared with the background frequency. It is seen that there is a discontinuity point on the spectral distribution, and the spectral distributions are asymmetric on the two sides of the point. This is quite different from the spectrum of the eye-shaped RW reported previously [22]. When $k = 1.8\ s$, the signal in component ψ_2 will evolve to be the anti-eye-shaped RW in Fig. 2(c), and the eye structure one in ψ_1 is kept as well. The corresponding spectrum evolutions are shown in Fig. 3(c) and 3(d). The valley on the lower frequency in Fig. 3(d) becomes much shallower than the one for the four-petaled flower RW. The spectrum corresponding to Fig. 3(a) and 3(c) is approaching the well-known symmetric triangular distribution [22]. When $k = 0$, the RW in each component becomes the standard

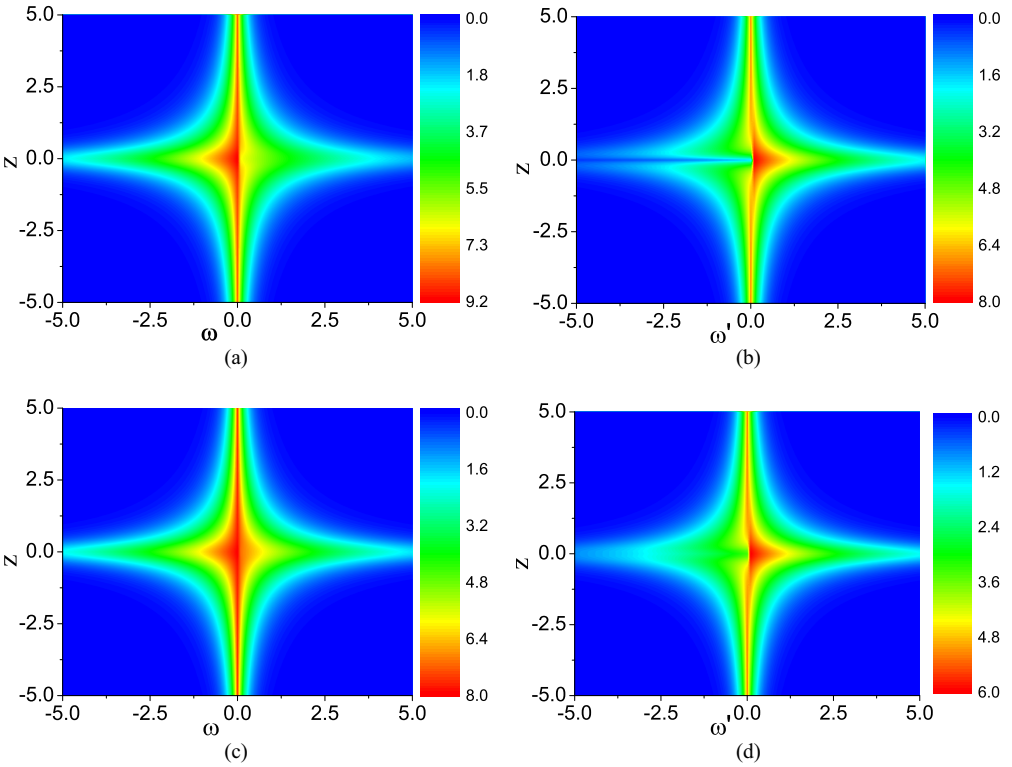

FIG. 3. (Color online) (a) The spectrum evolution $\sqrt{|F_1(\omega,z)|}$ of the RW in component ψ_1. (b) The spectrum evolution $\sqrt{|F_2(\omega',z)|}$ (where $\omega' = \omega + 1.1$) of the RW with the four-petaled flower structure in Fig. 1(c). (c) The spectrum evolution $\sqrt{|F_1(\omega,z)|}$ of the RW in component ψ_1. (d) The spectrum evolution $\sqrt{|F_2(\omega',z)|}$ (where $\omega' = \omega + 1.8$) of the RW with anti-eye structure in Fig. 2(c).

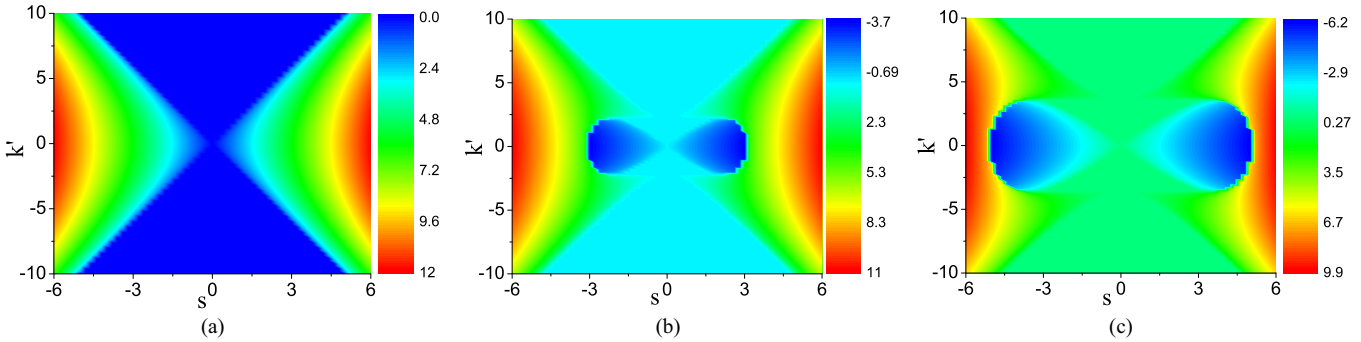

FIG. 4. (Color online) The modulational instability spectrum of the coupled system with relative wave vector $k = 0$ (a), $k = 1.1$ (b), and $k = 1.8$ (c).

eye-shaped one, whose spectrum is identical with the triangular spectrum of a Peregrine RW. In this way, we provide the spectrum relations between these different structured RWs. Then, why do we find these different patterns for RWs in the coupled nonlinear system?

It is known that MI can be seen as a mechanism for RWs in nonlinear systems. Therefore, relative frequency should play nontrivial role in the MI of the coupled system. We perform the linear instability analysis of plane wave backgrounds (ψ_{10} and ψ_{20}) in the system; namely, we add small-amplitude Fourier modes on the plane wave background as $\psi_1 = \psi_{10}\{1 + f_+ \exp[i\,k'(t - \Omega z)] + f_-^* \exp[-i\,k'(t - \Omega^* z)]\}$ and $\psi_2 = \psi_{20}\{1 + g_+ \exp[i\,k'(t - \Omega z)] + g_-^* \exp[-i\,k'(t - \Omega^* z)]\}$ (where f_+, f_-, g_+, and g_- are small amplitudes of the Fourier modes). Substituting them in Eq. (1) and after linearizing the equations, one can get the following dispersion relation:

$$-2k'^2\left(2s_1^2 + 2k^2 - 2k\Omega + 2s_2^2 + \Omega^2\right) + 4s_1^2(\Omega - 2k)^2 + k'^4 + \Omega^2\left(4k^2 - 4k\Omega + 4s_2^2 + \Omega^2\right) = 0. \quad (8)$$

We can demonstrate the instability regime Im(Ω) on the perturbation frequency k' vs amplitude of the backgrounds $s_1 = s_2 = s$ with different k values in Fig. 4. The coupled nonlinear system with these different relative frequencies $k = 0$ s, $k = 1.1$ s, and $k = 1.8$ s admits the eye-shaped RW pattern, four-petaled flower structure [Fig. 1 (c)], and anti-eye-shaped one [Fig. 2 (c)], respectively. It is seen that different MI gain spectrum characteristics correspond to different RW patterns. This partly means that different RW pattern types could come from the different MI gain spectra. It should be noted that the explanations for a dark RW in Ref. [25] cannot apply to the RWs obtained here, since there is no singularity for rational solution in coupled focusing NLS. We demonstrate qualitatively that different MI gain distribution properties induce different RW excitation patterns. Recently studies of the rational solution of the Sasa-Satsuma equation suggested that the dynamics of the rational solution can be understood well by its MI property. When the background frequency is in the MI regime, the rational solution corresponds to RW behavior [26,27]; otherwise, the rational solution demonstrates W-shaped soliton behavior [28] for the nonlnear fiber with high-order effects. It was also demonstrated that relative frequency can vary MI properties and induced RWs in coupled defocusing NLS [29]. However, the precise connections between them are still unknown, since the MI is qualitative to analyze but the RW solutions are exact and quantitative results for the nonlinear coupled model.

V. DISCUSSION AND CONCLUSION

In summary, we find that the two-component coupled model admits a RW with a four-petaled flower structure, in addition to an eye-shaped one and an anti-eye-shaped one. We demonstrate that these different RW patterns can be transited to each other through varying the relative frequency between the two modes. It can be expected that similar effects exist widely in multicomponent coupled systems. Furthermore, the spectra of different RW patterns are investigated exactly through performing a Fourier transformation. It is shown that the spectra of RWs with four-petaled flower and anti-eye shapes are asymmetric, in contrast to the symmetric distribution of a scalar Peregrine RWs' spectrum. The asymmetric character comes from the difference between the frequencies of the two-component backgrounds and cross-phase modulation effects, which are absent in the reported RW patterns in a scalar NLS system.

Scalar Akhmediev breathers, RWs, and Kuznetsov-Ma breathers have been excited successfully in nonlinear fiber [1,30]. Vector solitons have been realized in multi-component Bose-Einstein condensate systems [12] and in a nonlinear birefringent fiber [13]. It could be expected the the pattern transition can be observed experimentally in a nonlinear two-mode fiber or multicomponent Bose-Einstein condensate system through combining the techniques. These exact results would provide ideal initial conditions for these RW patterns of experimental excitations in vector nonlinear systems, including phase and intensity forms. By varying the frequency difference value, the pattern transition can be observed conveniently, combining with the corresponding initial excitation form construction. For example, we demonstrate an explicit parameter condition for a dark four-petaled flower RW in a nonlinear fiber with group velocity dispersion coefficient $\beta_2 = -20$ ps^2 km^{-1} and Kerr nonlinear coefficient $n_2 = 1.1$ W^{-1} km^{-1} for optical fields near wavelength 1.55 μm. When the mean intensity power is 1 W, the frequency difference should be 0.258 ps^{-1} to excite the four-petaled RW [Fig. 1 (c)] with the initial input profile given by the exact analytical solution. In fact, these conditions are given assuming that the system coefficients are identical for the two modes in the nonlinear fiber. Therefore, the frequency difference cannot

be too large to make the approximation unreasonable. Recent numerical and experimental studies suggest that the Peregrine RW can still be observed in a nonlinear system even with nonideal initial perturbations [31,32]. These patterns would also emerge in the vector nonlinear system even with some deviations from the ideal initial form.

Very recently studies of RWs in the nonlinear coupled system also showed that the relative frequency plays an important role in determining the RW structure, mainly including the long-wave-short-wave resonance equation [25] and coupled defocusing NLS [29]. Here we demonstrate the different pattern structures of RWs in coupled focusing NLS can be transited to each other by varying the relative frequency between the two modes.

ACKNOWLEDGMENT

This work is supported by National Science Foundation of China (Contact Nos. 11405129, 11347025).

APPENDIX: EXPLICIT EXPRESSIONS OF $\Phi_j(j = 1,2,3)$

The explicit expressions of $\Phi_j(j = 1,2,3)$ in Eqs. (5) and (6) are

$$\Phi_1[t,z] = -\frac{1}{3}A_3\ K(t,z),$$
$$\Phi_2[t,z] = \frac{iA_3s_1}{\lambda - k + 3i\tau}\left[\frac{9i}{\lambda - k + 3i\tau} + K(t,z)\right],$$
$$\Phi_3[t,z] = \frac{iA_3s_2}{\lambda + 2k + 3i\tau}\left[\frac{9i}{\lambda + 2k + 3i\tau} + K(t,z)\right],$$

where $K(t,z) = 2kz - 2\lambda z - 6iz\tau - 3t - 3$, and the parameter τ is

$$\tau = \frac{i\left[2\lambda^3 + \left(-3k^2 + 9s_1^2 + 9s_2^2\right)\lambda + 3k\lambda^2\right]}{2\left(3\lambda^2 + 3k^2 + 3\lambda k + 9s_1^2 + 9s_2^2\right)} - i\frac{2k^3 - 18ks_1^2 + 9ks_2^2}{2\left(3\lambda^2 + 3k^2 + 3\lambda k + 9s_1^2 + 9s_2^2\right)}.$$

The parameter λ which mainly determines the form of initial signals should satisfy the equation as

$$27k^2\lambda^4 + 54k\left(k^2 - s_1^2 + s_2^2\right)\lambda^3 + 27\left[k^4 + 2k^2\left(s_1^2 + 4s_2^2\right) + \left(s_1^2 + s_2^2\right)^2\right]\lambda^2$$
$$+54k\left[k^2\left(4s_1^2 + s_2^2\right) - 4s_1^4 + s_1^2s_2^2 + 5s_2^4\right]\lambda + 4\left(k^2 + 3s_1^2 + 3s_2^2\right)^3 - \left(2k^3 - 18ks_1^2 + 9ks_2^2\right)^2 = 0.$$

[1] B. Kibler, J. Fatome, C. Finot, G. Millot *et al.*, Nature Phys. **6**, 790 (2010).

[2] A. Chabchoub, N. P. Hoffmann, and N. Akhmediev, Phys. Rev. Lett. **106**, 204502 (2011).

[3] H. Bailung, S. K. Sharma, and Y. Nakamura, Phys. Rev. Lett. **107**, 255005 (2011).

[4] M. Onorato, S. Residori, U. Bortolozzo, A. Montina, and F. T. Arecchi, Phys. Rep. **528**, 47 (2013).

[5] A. R. Osborne, Mar. Struct. **14**, 275 (2001); N. Akhmediev, A. Ankiewicz, and M. Taki, Phys. Lett. A **373**, 675 (2009).

[6] N. Akhmediev, A. Ankiewicz, and J. M. Soto-Crespo, Phys. Rev. E **80**, 026601 (2009).

[7] L. C. Zhao and J. Liu, J. Opt. Soc. Am. B **29**, 3119 (2012).

[8] L. C. Zhao and J. Liu, Phys. Rev. E **87**, 013201 (2013).

[9] F. Baronio, M. Conforti, A. Degasperis, and S. Lombardo, Phys. Rev. Lett. **111**, 114101 (2013).

[10] D. R. Solli, C. Ropers, P. Koonath, and B. Jalali, Nature (London) **450**, 1054 (2007).

[11] D. R. Solli, C. Ropers, and B. Jalali, Phys. Rev. Lett. **101**, 233902 (2008); D. R. Solli, B. Jalali, and C. Ropers, *ibid.* **105**, 233902 (2010).

[12] C. Hamner, J. J. Chang, P. Engels, and M. A. Hoefer, Phys. Rev. Lett. **106**, 065302 (2011).

[13] D. Y. Tang, H. Zhang, L. M. Zhao, and X. Wu, Phys. Rev. Lett. **101**, 153904 (2008).

[14] Z. Y. Yan, Phys. Lett. A **375**, 4274 (2011).

[15] F. Baronio, A. Degasperis, M. Conforti, and S. Wabnitz, Phys. Rev. Lett. **109**, 044102 (2012).

[16] B. L. Guo and L. M. Ling, Chin. Phys. Lett. **28**, 110202 (2011).

[17] L. M. Ling, B. L. Guo, and L. C. Zhao, Phys. Rev. E **89**, 041201(R) (2014).

[18] Y. Ohta and J. K. Yang, Proc. R. Soc. A **468**, 1716 (2012).

[19] B. L. Guo, L. M. Ling, and Q. P. Liu, Phys. Rev. E **85**, 026607 (2012); Stud. Appl. Math. **130**, 317 (2013).

[20] J. S. He, H. R. Zhang, L. H. Wang, K. Porsezian, and A. S. Fokas, Phys. Rev. E **87**, 052914 (2013).

[21] L. M. Ling and L. C. Zhao, Phys. Rev. E **88**, 043201 (2013).

[22] N. Akhmediev, A. Ankiewicz, J. M. Soto-Crespo, and J. M. Dudley, Phys. Lett. A **375**, 541 (2011).

[23] B. Frisquet, A. Chabchoub, J. Fatome, C. Finot, B. Kibler, and G. Millot, Phys. Rev. A **89**, 023821 (2014).

[24] K. Hammani, B. Wetzel, B. Kibler, J. Fatome *et al.*, Opt. Lett. **36**, 2140 (2011).

[25] S. H. Chen, P. Grelu, and J. M. Soto-Crespo, Phys. Rev. E **89**, 011201(R) (2014).
[26] U. Bandelow and N. Akhmediev, Phys. Rev. E **86**, 026606 (2012).
[27] S. H. Chen, Phys. Rev. E **88**, 023202 (2013).
[28] L. C. Zhao, S. C. Li, and L. M. Ling, Phys. Rev. E **89**, 023210 (2014).
[29] F. Baronio, M. Conforti, A. Degasperis, S. Lombardo, M. Onorato, and S. Wabnitz, Phys. Rev. Lett. **113**, 034101 (2014).
[30] B. Kibler, J. Fatome, C. Fnot, G. Millot, G. Genty *et al.*, Sci. Rep. **2**, 463 (2012).
[31] G. Y. Yang, L. Li, and S. T. Jia, Phys. Rev. E **85**, 046608 (2012).
[32] J. M. Dudley, G. Genty, F. Dias *et al.*, Opt. Express **17**, 21497 (2009).